Optimizing the thermoelectric efficiency of icosahedral quasicrystals and related complex alloys

Enrique Maciá*
Dpto. Física de Materiales, Facultad CC. Físicas, Universidad Complutense de Madrid, E-28040 Madrid, Spain
(Received 29 June 2009; revised manuscript received 4 September 2009; published 3 November 2009)

In this work we analyze the potential role of quasicrystals and related alloys in thermoelectric material research. Relatively large figure of merit values are expected for those samples exhibiting two properly located narrow features in the density of states close to the Fermi level. It is expected that optimized quasicrystals will perform better at relatively low temperatures, whereas the *ZT* curve of complex metallic alloys reaches its maximum at high temperatures. Among state-of-the-art quasicrystals most promising samples for thermoelectric applications are found in the AlPd(Mn,Re) system. Quasicrystalline and related approximants in the ScMgCuGa and CaAuIn systems, synthesized on the basis of pseudogap tuning concepts, appear as promising candidates as well.

DOI: 10.1103/PhysRevB.80.205103 PACS number(s): 61.44.Br, 71.20.−b, 72.10.−d

I. INTRODUCTION

The efficiency of thermoelectric materials (TEMs) for energy conversion or electronic refrigeration depends on their transport coefficients and it can be evaluated in terms of the figure of merit (FOM) given by the dimensionless expression

$$ZT \equiv \frac{P(T)}{\kappa_e(T) + \kappa_l(T)} T, \tag{1}$$

where T is the temperature, $P(T) \equiv \sigma(T) S^2(T)$ is the so-called thermoelectric power factor, $\sigma(T)$ is the electrical conductivity, $S(T)$ is the Seebeck coefficient, and $\kappa_e(T)$ and $\kappa_l(T)$ are the charge carrier and lattice contributions to the thermal conductivity, respectively. In order to optimize *ZT* one then must search for materials exhibiting large power factors and low thermal conductivities, preferably governed by their lattice contribution (i.e., $\kappa_l \gg \kappa_e$). This explains the traditional interest in narrow gap semiconductors in the quest for good TEMs, the BiTe alloy family being the most widely used TEM at room temperature ($ZT \simeq 0.7$).[1]

Quasicrystals (QCs) are metallic alloys, representative of a novel condensed matter phase which can be regarded as a natural extension of the notion of a crystal to structures with quasiperiodic, rather than periodic, long-range order. Thus, QCs show an essentially discrete diffraction pattern (typical of well-ordered systems), although exhibiting unusual symmetry arrangements of the diffraction spots, related to icosahedral, octogonal, decagonal, and dodecagonal symmetries.[2,3] Shortly after the discovery of thermodynamically stable QCs of high structural quality in the Al-Cu(Fe,Ru,Os), AlPd(Mn,Re), ZnMg(RE), and Cd(Yb,Ca) icosahedral systems,[4] it was progressively realized that these materials occupy an odd position among the well-ordered condensed matter phases. In fact, since QCs consist of metallic elements one would expect they should behave as metals. Nonetheless, it is now well established that transport properties of stable QCs are quite unusual by the standard of common metallic alloys, as most of their transport properties resemble a more semiconductorlike than metallic character.[2,3] For the sake of comparison in Table I we list a number of characteristic physical properties of both metals and QCs. By inspecting this table one realizes that quasicrystalline alloys significantly depart from metallic behavior, resembling either ionic or semiconducting materials. Thus, high-quality QCs provide an intriguing example of solids made of typical metallic atoms which do not exhibit most of the physical properties usually signaling the presence of metallic bonding.

For instance, their electrical conductivity (1) is remarkably low, ranging from about 10^2 to 10^4 $\Omega^{-1}\,\mathrm{cm}^{-1}$ at room temperature, (2) steadily *increases* as the temperature increases up to the melting point, and (3) is extremely sensitive to minor variations in the sample composition, resembling doping effects in semiconductors. In addition, QCs bearing transition metals in the systems *i*-AlCu(Fe,Ru,Os) and *i*-AlPd(Mn,Re) exhibit significantly large thermoelectric power values (30–120 $\mu\mathrm{V}\,\mathrm{K}^{-1}$) as compared to those of typical metallic systems (1–10 $\mu\mathrm{V}\,\mathrm{K}^{-1}$) at room temperatures, and the temperature dependence of the Seebeck coefficient usually deviates from the linear behavior (characteristic of electron diffusion in ordinary metallic alloys), exhibiting pronounced curvatures at temperatures above ~50–100 K. Furthermore, the thermal conductivity of QCs is about two orders of magnitude lower than that of common

TABLE I. Comparison between the physical properties of quasicrystalline alloys versus typical metallic materials. I (S) stands for ionic (semiconducting) material typical properties.

Property	Metals	Quasicrystals
Mechanical	Ductility, malleability	Brittle (I)
Tribological	Relatively soft	Very hard (I)
	Easy corrosion	Corrosion resistant
Electrical	High conductivity	Low conductivity (S)
	Resistivity increases with T	Resistivity decreases with T (S)
	Small thermopower	Large thermopower (S)
Magnetic	Paramagnetic	Diamagnetic
Thermal	High conductivity	Very low conductivity (I)
	Large specific heat	Small specific heat
Optical	Drude peak	No Drude peak, IR absorption (S)

TABLE II. Room temperature values of the transport coefficients and FOM for several *i*-AlPdRe samples reported in the literature (Ref. 7) arranged according to their electron per atom ratio e/a.

Sample	e/a	σ (Ω^{-1} cm^{-1})	S (μV K^{-1})	P (μW m^{-1} K^{-2})	κ (W m^{-1} K^{-1})	ZT
$Al_{68.5}Pd_{22.9}Re_{8.6}$	1.740	110	−10	1.1	1.16	0.0003
$Al_{69.4}Pd_{21.2}Re_{9.4}$	1.738	95	−7	0.5	1.2[a]	0.0001
$Al_{67.7}Pd_{23.2}Re_{9.1}$	1.698	90	55	27.2	0.86	0.01
$Al_{67.8}Pd_{22.2}Re_{10.0}$	1.668	180	95	162.5	0.76	0.06

[a]Estimated.

metals, within the range of ~1–5 W m^{-1} K^{-1} at room temperature, and it is mainly determined by the lattice phonons, rather than by the charge carriers, over a wide temperature range. This property is particularly remarkable in the light of Slack's phonon-glass and electron-crystal proposal for promising TEMs.[5] In summary, according to Eq. (1) the unusual behaviors reported for both the electronic and thermal transport properties, when taken together, clearly favor a FOM enhancement. Therefore, QCs occupy a very promising position in the quest for novel TEMs, naturally bridging the gap between semiconducting materials and metallic ones.[6]

II. PHYSICAL MOTIVATIONS

The main advantage of QCs is that one can efficiently exploit the high sensitivity of their transport coefficients to stoichiometric changes in order to properly enhance their power factors, thereby optimizing the numerator in Eq. (1), without sacrificing their characteristic low thermal conductivity. This property is illustrated in Table II, where we list the power factor and FOM values for several *i*-AlPdRe representatives. The samples are listed according to the value of the so-called average electron per atom ratio, e/a, which is obtained from their stoichiometric composition by assuming the valence values Al=+3, Pd=0, and Re=−3.66. In so doing, one generally assumes that the Hume-Rothery mechanism plays a substantial role in QC stabilization, and the transition atoms take electrons from the conduction band, hence adopting a negative effective valence.[8,9] As we can see, P and ZT values differing by more than two orders of magnitude can be attained in a single QC system by slightly changing the sample's composition by a few atomic percent (hence preserving the quasiperiodic crystalline structure). We also note that both positive and negative values of the thermopower can be obtained in this way, which allows for both the *n*- and *p*-type legs in a typical thermoelectric cell to be fabricated from the same material.[10]

In Table III we list the transport coefficients and thermoelectric response data for those representatives of the different QC families yielding the best FOM values at room temperature. By inspecting this table two main conclusions can be drawn: (1) typically metallic, very small ZT values are obtained for those QCs exhibiting either $e/a \simeq 1.75$ or $e/a \simeq 2.00$; (2) isostructural i-$Al_{71}Pd_{20}(Re,Mn)_9$ samples, with $e/a \simeq 1.80$, exhibit the largest ZT values. Furthermore, significantly enhanced FOM values are obtained at higher temperatures for closely related QCs exhibiting similar e/a values. Thus we have $ZT=0.26$ for i-$Al_{68}Ga_3Pd_{20}Mn_9$ samples at $T=473$ K,[16] $ZT=0.23$ for i-$Al_{70.8}Pd_{20.9}Mn_{8.3}$ samples ($e/a=1.820$) at $T=550$ K,[10] $ZT=0.21$ for $Al_{71}Pd_{20}(Re_{0.35}Fe_{0.65})_9$ samples ($e/a=1.859$) at $T=500$ K,[18] and $ZT=0.15$ for i-$Al_{71}Pd_{20}Re_9$ samples and i-$Al_{71}Pd_{20}(Re_{0.45}Ru_{0.55})_9$ samples ($e/a=1.850$) at $T=570$ K

TABLE III. Room temperature values of the transport coefficients and FOM for QCs belonging to different families as reported in the literature. The e/a ratio has been obtained by assuming the valences Cu=+1, Ag=+1, Mg=+2, Cd=+2, Zn=+2, Yb=+2, In=+3, Ga=+3, Er=+3, Si=+4, Mn=−3.66, Fe=−2.66, and Ru=−2.66.

Sample	Ref.	e/a	σ (Ω^{-1} cm^{-1})	S (μV K^{-1})	P (μW m^{-1} K^{-2})	κ (W m^{-1} K^{-1})	ZT
$Zn_{57}Mg_{34}Er_9$	11	2.090	6170	7	30	4.5	0.002
$Al_{65}Cu_{20}Ru_{15}$	12	1.751	250	27	19	1.8[a]	0.003
$Ag_{42.5}In_{42.5}Yb_{15}$	13	2.000	5140	12	74	4.8	0.005
$Al_{62.5}Cu_{24.5}Fe_{13}$	12	1.774	310	44	60	1.8[b]	0.01
$Cd_{84}Yb_{16}$	14	2.000	7000	16	179	4.7	0.01
$Al_{64}Cu_{20}Ru_{15}Si_1$	12	1.761	390	50	98	1.8[a]	0.02
$Al_{71}Pd_{20}Re_9$	15	1.801	450	80	288	1.3	0.07
$Al_{71}Pd_{20}Mn_9$	16	1.801	714	90	578	1.5	0.12

[a]Estimated upper limit.
[b]After Ref. 17.

(Ref. 15) and $T=700$ K,[19] respectively. On the other hand, FOM values similar to those of *i*-AlPd(Re,Mn) samples have been reported for the cubic approximant phases 1/1-$Al_{71.6}Re_{17.4}Si_{11}$ ($e/a=1.951$, $ZT=0.10$) and 1/1-$Al_{75.6}Mn_{17.4}Si_7$ ($e/a=1.911$, $ZT=0.07$) at room temperatures.[20] These crystals have not only very similar compositions in the phase diagram but also structures closely resembling that of related QCs and exhibit most of their characteristic transport property anomalies as well.

These experimental results clearly highlights the important role of band structure effects in the thermoelectric response of QCs and related alloys, suggesting that additional improvement may be attained by a judicious choice of both sample composition and processing conditions. In fact, some time ago it was proposed on sound theoretical basis that the best TEM is likely to be found among materials exhibiting a sharp singularity in the density of states (DOS) close to the Fermi level, and that the larger the DOS value at the Fermi level, the smaller the FOM value at low temperatures.[21] Quite interestingly the electronic structure of QCs fits in this framework in a natural way since their electronic structure is characterized by two main contributions: (1) a *pronounced pseudogap* at the Fermi level[2,22] and (2) several *narrow* spectral features in the DOS near the Fermi level.[23,24]

III. PHENOMENOLOGICAL APPROACH

Inspired by these physical motivations we have undertaken a prospective theoretical study on the potential of different QCs and related alloys as TEMs on the basis of their peculiar electronic structure.[6,25–28] In order to make a meaningful comparison with experimental measurements one should take into account possible finite lifetime and temperature broadening effects. In so doing, it is observed that most finer details in the DOS are significantly smeared out and only the most conspicuous peaks remain in the vicinity of the Fermi level at room temperature.[29] These considerations convey us to reduce the number of main spectral features necessary to capture the most relevant physics of the transport processes. Following previous works we consider a realistic model for the electronic structure of transition metal bearing, Al-based *i*-QCs, and related phases in terms of the spectral conductivity function (defined as the $T\rightarrow 0$ conductivity with the Fermi level at energy E) given by[30]

$$\sigma(E)=\bar{\sigma}\left\{\frac{\gamma_1}{(E-\delta_1)^2+\gamma_1^2}+\frac{\alpha\gamma_2}{(E-\delta_2)^2+\gamma_2^2}\right\}^{-1}. \quad (2)$$

This model includes six parameters, determining Lorentzian's heights ($\bar{\sigma}/\gamma_i$) and widths ($\sim\gamma_i$), their positions with respect to the Fermi level, δ_i, and their relative weight in the overall structure, $\alpha>0$. The parameter $\bar{\sigma}$ is a scale factor measured in $(\Omega\ \mathrm{cm\ eV})^{-1}$ units. The overall behavior of this curve (see Fig. 1) agrees well with the experimental results obtained from tunneling and point contact spectroscopy measurements, where the presence of a dip feature of small width (20–60 meV), superimposed onto a broad (0.5–1 eV) asymmetric pseudogap, has been reported.[23,31–33] Thus, Eq. (2) satisfactorily describes the electronic structure of these alloys

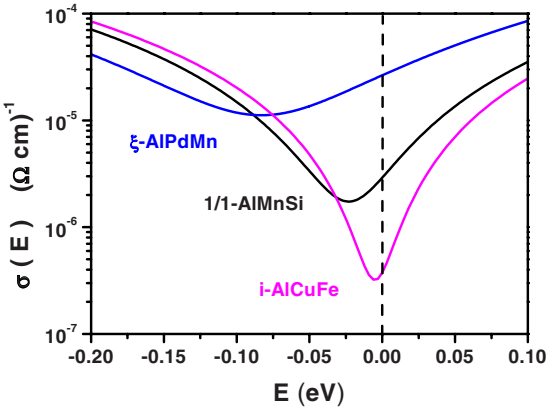

FIG. 1. (Color online) Spectral conductivity function curves corresponding to the electronic model parameters listed in Table V for the *i*-$Al_{63}Cu_{25}Fe_{12}$, 1/1-$Al_{73.6}Mn_{17.4}Si_9$, and ξ-$Al_{73}Pd_{22.9}Mn_{4.1}$ samples. The dashed vertical line indicates the Fermi level position.

in terms of a wide Lorentzian peak (related to the Fermi surface–Brillouin zone interaction) plus a narrow Lorentzian peak (related to *sp-d* hybridization effects).[8,9] In this regard, it is important to note that the resulting narrow dip at the center of the pseudogap mainly stems from the Hume-Rothery mechanism and it is only marginally related to the possible existence of long-range order, quasiperiodicity related spiky features in the DOS. This spiky component (over an energy scale of about 10 meV) is still awaiting for a definitive experimental confirmation, as it was originally obtained from self-consistent *ab initio* calculations,[34] and the very nature of its physical origin has been extensively debated in the literature.[35–39] Suitable values for the electronic model parameters appearing in Eq. (2) can be obtained by properly combining *ab initio* calculations with experimental transport data within a phenomenological approach previously described.[3,40–42] Note that in the limit $\alpha\rightarrow 0$ (i.e., the model narrow feature becomes negligible) the spectral conductivity function given by Eq. (2) adopts a simple parabolic form around the Fermi level and the temperature dependence of the transport coefficient obtained from Eqs. (8)–(10) exhibits a typically metallic behavior. Accordingly, the presence of the second spectral feature in Eq. (2) is necessary in order to properly account for the unusual transport properties reported in QCs and related alloys.

The temperature-dependent transport coefficients can be obtained from the knowledge of the spectral conductivity function by means of the Kubo-Greenwood version of the linear response theory. Within this approach the electrical, $\mathbf{j}$, and thermal, $\mathbf{h}$, current densities are related to the voltage and temperature gradients, respectively, according to the expression

$$\begin{pmatrix}\mathbf{j}\\ \mathbf{h}\end{pmatrix}=\begin{pmatrix}\mathcal{L}_{11} & \mathcal{L}_{12}\\ \mathcal{L}_{21} & \mathcal{L}_{22}\end{pmatrix}\begin{pmatrix}-\nabla V\\ -\nabla T\end{pmatrix}. \quad (3)$$

The central information quantities are the kinetic coefficients

$$\mathcal{L}_{ij}(T)=(-1)^{i+j}\int\sigma(E)(E-\mu)^{i+j-2}\left(-\frac{\partial f}{\partial E}\right)dE, \quad (4)$$

where $f(E,\mu,T)$ is the Fermi-Dirac distribution function, E is the electron energy, and μ is the chemical potential. In this

TABLE IV. Thermoelectric figure of merit at $T=10^3$ K for several complex metallic alloys calculated from their electronic structure model parameters making use of Eq. (15). The cubic approximant phase AlMnSi has a unit-cell volume of 2 nm^{-3}, containing $N=138$ atoms. The ξ- and Ψ-AlPdMn phases have an orthorhombic unit-cell composed of Mackay clusters as basic building blocks. Their unit-cell volume are $V=4.81$ nm^3 and $V=22.22$ nm^3, containing $N=320$ and $N=1500$ atoms, respectively (Ref. 2).

Sample	Ref.	α	δ_1 (meV)	δ_2 (meV)	γ_1 (meV)	γ_2 (meV)	ZT
i-$Al_{63}Cu_{25}Fe_{12}$	27	1.07	−5	−16	587	55	0.001
1/1-$Al_{73.6}Mn_{17.4}Si_9$	40	0.21	23	−29	65	22	0.015
ξ-$Al_{73}Pd_{22.9}Mn_{4.1}$	This work	0.72	83	−72	134	85	0.046
Ψ-$Al_{72.9}Pd_{22.9}Mn_{4.2}$	42	0.83	102	−50	86	81	0.049

formulation all the microscopic details of the system are included in the $\sigma(E)$ function. From the knowledge of the kinetic coefficients one obtains the electrical conductivity

$$\sigma(T)=\mathcal{L}_{11}(T), \tag{5}$$

the thermoelectric power

$$S(T)=\frac{1}{|e|T}\frac{\mathcal{L}_{12}(T)}{\sigma(T)}, \tag{6}$$

and the electronic thermal conductivity

$$\kappa_e(T)=\frac{1}{e^2T}\mathcal{L}_{22}(T)-T\sigma(T)S(T)^2 \tag{7}$$

in a unified way. Then, by expressing Eqs. (5)–(7) in terms of the scaled variable $x\equiv(E-\mu)\beta$, where $\beta\equiv(k_BT)^{-1}$, the transport coefficients can be rewritten as

$$\sigma(T)=\frac{J_0}{4}, \tag{8}$$

$$S(T)=-\frac{k_B}{|e|}\frac{J_1}{J_0}, \tag{9}$$

$$\kappa_e(T)=\frac{T}{c^2J_0}\begin{vmatrix} J_0 & J_1 \\ J_1 & J_2 \end{vmatrix} \tag{10}$$

in terms of the reduced kinetic coefficients, where $c\equiv 2e/k_B$,

$$J_n=\int_{-\infty}^{\infty}x^n\sigma(x)\mathrm{sech}^2(x/2)dx. \tag{11}$$

Plugging Eqs. (8)–(10) into Eq. (1) one gets

$$ZT=\frac{J_1^2}{J_0J_2-J_1^2+c^2J_0\varphi}, \tag{12}$$

where $\varphi(T)\equiv\kappa_l(T)/T$. Making use of Eq. (2) the kinetic coefficients can be expressed in the polynomial form,[42]

$$J_0=A\left(J_{00}+J_{02}\beta^{-2}+\sum_{n=2}^{\infty}J_{0,2n}\beta^{-2n}\right),$$

$$J_1=A\left(J_{11}\beta^{-1}+\sum_{n=2}^{\infty}J_{1,2n-1}\beta^{-2n+1}\right),$$

$$J_2=A\left(J_{20}+J_{22}\beta^{-2}+\sum_{n=3}^{\infty}J_{2,2(n-1)}\beta^{2(1-n)}\right), \tag{13}$$

where $3A\equiv 4\pi^2\bar{\sigma}(\gamma_1+\alpha\gamma_2)^{-1}$ and the coefficients J_{ij} only depend on the electronic model parameters $\{\gamma_i,\delta_i,\alpha\}$. In the low temperature regime the kinetic coefficients reduce to the zeroth-order terms in Eqs. (13) and $\kappa_l\sim T^3$, so that the $c^2J_0\varphi\sim T^2$ and $J_1^2\sim T^2$ terms become negligible with respect to the J_0J_2 constant term in Eq. (12) and we get $ZT\simeq 4b\xi_1^2T^2$, where $b\equiv\pi^2k_B^2/3=2.44\times10^{-8}$ eV^2 K^{-2} and

$$\xi_1\equiv-\frac{\gamma_1\delta_1\varepsilon_2^4+\alpha\gamma_2\delta_2\varepsilon_1^4}{\varepsilon\varepsilon_1^4\varepsilon_2^4}=\frac{1}{2}\left(\frac{d\ln\sigma(E)}{dE}\right)_{E_F} \tag{14}$$

measures the slope of the DOS close to E_F, where $\varepsilon\equiv\gamma_1\varepsilon_1^{-2}+\alpha\gamma_2\varepsilon_2^{-2}$ and $\varepsilon_i^2=\gamma_i^2+\delta_i^2$.[40] On the other hand, at high enough temperatures we have[42] $J_0\to Ak_B^2T^2$, $J_1\to Aa_1k_BT$, $J_2\to 21AbT^2/5$, and $\kappa_l\to 0$, so that the term $J_0J_2\sim T^4$ dominates the denominator of Eq. (12), and we obtain

$$ZT=\frac{20}{21b}\left(\frac{\gamma_1\delta_1+\alpha\gamma_2\delta_2}{\gamma_1+\alpha\gamma_2}\right)^2\frac{1}{T^2}. \tag{15}$$

The reliability of Eq. (15) can be estimated from the high-temperature ZT values derived from the electronic model parameters listed in Table IV for suitable representatives of QCs and related metallic alloys exhibiting complex structures. In fact, these values compare well with the experimentally reported high-temperature ZT values corresponding to the samples i-$Al_{71}Pd_{20}Mn_9$ ($ZT\simeq 0.02$ at $T=973$ K) (Ref. 16) and i-$Al_{71}Pd_{20}Re_9$ ($ZT\simeq 0.05$ at $T=950$ K).[18]

Since ZT is a continuous function of T, the functional dependence of the FOM in the low- and high-temperature limits guarantees that ZT must attain a maximum value at some intermediate temperature. According to several transport measurements $\kappa_l\sim T^n$ (with $n=1.2-1.7$ in the 100–300 K interval),[42] whereas $\kappa_e\sim T^3$ above 200 K,[43] so that the ratio $\kappa_l/\kappa_e\sim T^{-3/2}$ progressively reduces as the temperature increases. By expressing Eq. (1) in the form

TABLE V. Thermoelectric figure of merit at the best performance temperature T_* obtained from Eq. (17) along with the corresponding refined electronic structure model parameters derived from the values listed in Table IV (for more details see the text).

Sample	$\tilde{\alpha}$	$\tilde{\delta}_1$ (meV)	$\tilde{\delta}_2$ (meV)	$\tilde{\gamma}_1$ (meV)	$\tilde{\gamma}_2$ (meV)	T_* (K)	ZT_*
i-$Al_{63}Cu_{25}Fe_{12}$	2.32	±5	±16	12	16	72	0.011
1/1-$Al_{73.6}Mn_{17.4}Si_9$	1.23	±23	±29	28	29	173	0.235
ξ-$Al_{73}Pd_{22.9}Mn_{4.1}$	0.86	±83	±72	71	72	471	0.299

$$ZT = \left(\frac{J_0 J_2}{J_1^2} - 1\right)^{-1}\left(1 + \frac{k_l}{k_e}\right)^{-1}, \tag{16}$$

we realize that electronic structure effects play the major role in determining ZT in the intermediate temperature regime. Thus, by keeping terms up to β^{-2} in Eqs. (13), Eq. (16) takes the form

$$ZT = \frac{A_3 T^2}{1 + (A_1 - A_3)T^2 + \frac{105}{676}A_1^2 T^4}, \tag{17}$$

where $A_3 \equiv 4b\xi_1^2$ and $A_1 = 26bJ_{02}/(5J_{20})$. The largest ZT value will be obtained when $A_1 = A_3$, hence minimizing the denominator in Eq. (17). In that case the best performance temperature is given by $T_* = \sqrt{26/(A_3\sqrt{105})} \simeq 5100/|\xi_1|$ K, where ξ_1 is measured in eV^{-1}, leading to the optimal FOM value $ZT_* \simeq 1.27$. This is a significantly large figure compared to those reported for current benchmark TEMs. The value of ξ_1 can be experimentally determined from the Seebeck coefficient slope at low temperatures from the expression $S(T) \simeq -2|e|^{-1}b\xi_1 T$.[26] In this way, an empirical correlation between $|\xi_1|$ and ZT values was disclosed for a series of *i*-AlPdMn samples with different stoichiometric compositions.[44] In fact, the $ZT(\xi_1)$ curve exhibits a deep minimum, where ZT almost vanishes, at $e/a \simeq 1.74$, flanked by two maxima at about $\xi_1 \simeq -25$ eV^{-1} and $\xi_1 \simeq +40$ eV^{-1}. Then, the ZT overall behavior can be traced back to the topology of the spectral conductivity function close to the Fermi level by means of Eq. (14): when the Fermi level is located close to the pseudogap minimum, Eq. (14) yields very small ξ_1 values. In that case, one gets small figures of ZT at room temperature, in agreement with the experimental results, whereas as the Fermi level progressively shifts from the pseudogap's minimum, the ZT values progressively increase attaining well-defined maxima.

IV. ELECTRONIC STRUCTURE REFINEMENT

In order to obtain convenient electronic structures we have optimized Eq. (14), under the physical restrictions $\alpha > 0$ and $\gamma_i > 0$, to obtain the refined electronic model parameters $\tilde{\delta}_1 = \pm\delta$, $\tilde{\delta}_2 = \pm(\delta/2 + \epsilon)$, $\tilde{\gamma}_1 = \sqrt{2\delta\epsilon}$, $\tilde{\gamma}_2 = \delta/2 + \epsilon$, and $\tilde{\alpha} = \sqrt{2\epsilon/\delta}$ in terms of the reference values δ_1 and δ_2, where $\delta \equiv |\delta_1|$ and $\epsilon = |\delta_2| - |\delta_1|/2 > 0$. In Table V we present the refined electronic model parameters corresponding to the samples listed in Table IV along with their optimal FOM at the best performance temperature. By comparing Tables IV and V two main conclusions can be drawn. First, $\tilde{\alpha} > \alpha$ in all considered cases. This indicates that in the refined electronic structure the spectral feature related to *sp-d* hybridization effects plays a more significant role. Second, the widths of both spectral features become comparable to each other, hence indicating that the Fermi surface–Brillouin zone interaction becomes comparable to *sp-d* hybridization effects. Detailed *ab initio* band structure calculation showed that the half-width γ_i parameters of the spectral conductivity model can be related to the diffusivity of the corresponding states.[45,46] In fact, generally speaking the conductivity spectrum takes into account both the DOS structure, $N(E)$, and the diffusivity of the electronic states, $D(E)$, according to the relationship $\sigma(E) = e^2 N(E) D(E)$. Thus, although it may be tempting to assume that the $\sigma(E)$ function should closely resemble the overall structure of the DOS, it has been shown that a dip in the $\sigma(E)$ curve can correspond to a peak in the DOS at certain energies.[45,47] This behavior is likely to be related to the peculiar nature of critical electronic states close to the Fermi level.[3,48,49] Accordingly, the narrowing of the $\tilde{\gamma}_1$ parameter in the refined model can be interpreted as higher localization of electronic states induced by an enhancement in the covalent bonding nature in the cluster network,[50] in agreement with photoconductivity measurements.[51]

Note that optimizing ξ_1 is a necessary but not sufficient condition to attain the optimal ZT value characterized by $A_1 = A_3$ in Eq. (17). Accordingly, the FOMs reported in Table V are not the (ideally) best possible ones (though they actually improve the best records reported to date for the corresponding samples). In Fig. 1 the corresponding spectral conductivity functions are compared in an energy window close to the Fermi level. The $\sigma(E)$ curve of the *i*-QC is characterized by a pronounced pseudogap with steep wings and the Fermi level is very close to its dip. Both the depth and the width of the pseudogap progressively reduce as the atomic volume of the considered alloy decreases ($N/V = 66.53$ at nm^{-3} for ξ-$Al_{73}Pd_{22.9}Mn_{4.1}$ and $N/V = 69.0$ at nm^{-3} for 1/1-$Al_{73.6}Mn_{17.4}Si_9$) and the location of the pseudogap minimum progressively shifts below the Fermi level as well. The overall structure of the DOS close to the Fermi level is directly related to the thermoelectric performance of the corresponding sample, as it is illustrated in the ZT curves shown in Fig. 2. In fact, since ξ_1 depends on the slope of the DOS close to the Fermi level according to Eq. (14), the steeper the slope of the $\sigma(E)$ curve at E_F, the steeper the Seebeck coefficient (and consequently the ZT) curve at low temperatures. Accordingly, the *i*-QC exhibits a substantially larger FOM value than the other related phases in the low temperature

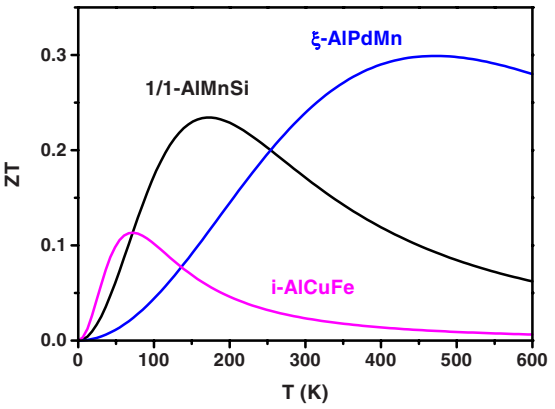

FIG. 2. (Color online) Temperature dependence of the thermoelectric figure of merit obtained from Eq. (17) making use of the electronic model parameters listed in Table V for the i-$Al_{63}Cu_{25}Fe_{12}$, 1/1-$Al_{73.6}Mn_{17.4}Si_9$, and ξ-$Al_{73}Pd_{22.9}Mn_{4.1}$ samples.

regime. This trend is reversed at higher temperatures, so that the best thermoelectric performance is now exhibited by the giant unit-cell ξ-$Al_{73}Pd_{22.9}Mn_{4.1}$ compound.

At this point some words are regarding the very possibility of tailoring the electronic structure properties of actual QCs and their related approximant phases in practice. As it is well known no definite guideline for the discovery of new QC systems has been found and the rules for tuning their electronic properties are far from being properly understood. Notwithstanding this, very promising results have been recently reported on the basis of pseudogap tuning concepts.[52] Within this framework one starts by choosing an appropriate trial sample candidate (e.g., a polar intermetallic Zintl phase) taking into account its crystal symmetry (according to the group-subgroup relationships), the existence of structural clusters with the appropriate fivefold symmetry, and the presence of a significant pseudogap in the DOS *below* the Fermi level. Then, the average electron per atom ratio is systematically changed by substituting metal cations by electron-richer elements (shifting the Fermi level toward the DOS minimum) of comparable ionic radius (hence preserving the structural network) having low-lying d orbitals (which favors the sp-d orbital mixing and bond formation). In this way, icosahedral QC and related approximants in the ScMgCuGa and CaAuIn systems have been obtained from the parent cubic crystals $Mg_2Cu_6Ga_5$ and $Na_2Au_6In_5$, respectively.[53] Since these compounds are synthesized following a well-defined band structure engineering process from the very beginning, it is reasonable to expect that the electronic structure refinement considered in the present work may be attainable (at some degree at least) in the years to come.

V. CONCLUSIONS

From the experimental data listed in Table III one realizes that the larger FOM values at room temperature obtained to date are those reported for samples belonging to the AlPd-(Mn,Re) system. The results obtained in this work indicate that improved thermoelectric properties may be expected in these materials by properly engineering the band structure close to the Fermi level. According to Fig. 2 one should expect that QCs perform better at low temperatures, whereas the ZT curve of complex unit-cell phases reaches its maximum at high temperatures. In addition to the AlPd(Mn,Re) phases (which have already been widely studied) the recently synthesized $Sc_{16}Mg_3Cu_{48}Ga_{33}$ and $Ca_{14}Au_{44}In_{42}$ icosahedral QCs (and related approximants) appear as quite natural candidates to explore the possibility of properly locating the main spectral features close to the Fermi level in order to obtain large ZT values though (to the best of my knowledge) the temperature dependence of the transport coefficients corresponding to these materials has not yet been reported.

ACKNOWLEDGMENTS

I warmly thank Kaoru Kimura, Tsunehiro Takeuchi, and Terry M. Tritt for sharing useful information and M. Victoria Hernández for a critical reading of the paper. This work has been supported by the Universidad Complutense de Madrid and Banco Santander through Project No. PR34/07-15824.

*emaciaba@fis.ucm.es

[1] *Recent Trends in Thermoelectric Materials Research*, Semiconductors and Semimetals Vol. 71, edited by T. M. Tritt (Academic Press, San Diego, 2001).
[2] J. M. Dubois, *Useful Quasicrystals* (World Scientific, Singapore, 2005).
[3] E. Maciá, *Aperiodic Structures in Condensed Matter: Fundamentals and Applications* (CRC Press, Boca Raton, FL, 2009).
[4] A. P. Tsai, in *Physical Properties of Quasicrystals*, Springer Series in Solid-State Physics Vol. 126, edited by Z. M. Stadnik (Springer, Berlin, 1999), p. 5.
[5] G. A. Slack, in *CRC Handbook of Thermoelectrics*, edited by D. M. Rowe (CRC Press, Boca Raton, FL, 1995).
[6] E. Maciá, Phys. Rev. B **64**, 094206 (2001).
[7] K. Kirihara and K. Kimura, J. Appl. Phys. **92**, 979 (2002).
[8] U. Mizutani, T. Takeuchi, and H. Sato, Prog. Mater. Sci. **49**, 227 (2004).
[9] G. Trambly de Laissardière, D. Nguyen-Manh, and D. Mayou, Prog. Mater. Sci. **50**, 679 (2005).
[10] A. L. Pope, B. M. Zawilski, R. Gagnon, T. M. Tritt, J. Ström-Olsen, R. Schneidmiller, and J. W. Kolis, in *Quasicrystals*, MRS Symposia Proceedings No. 643 (Materials Research Society, Pittsburgh, 2001), p. K14.4.1.
[11] K. Giannò, A. V. Sologubenko, M. A. Chernikov, H. R. Ott, I. R. Fisher, and P. C. Canfield, Mater. Sci. Eng., A **294-296**, 715 (2000).
[12] F. S. Pierce, P. A. Bancel, B. D. Biggs, Q. Guo, and S. J. Poon, Phys. Rev. B **47**, 5670 (1993).
[13] Y. K. Kuo, K. M. Sivakumar, H. H. Lai, C. N. Ku, S. T. Lin, and A. B. Kaiser, Phys. Rev. B **72**, 054202 (2005).

[14] Y. K. Kuo, H. H. Lai, C. H. Huang, W. C. Ku, C. S. Lue, and S. T. Lin, J. Appl. Phys. **95**, 1900 (2004).
[15] Y. Takagiwa, T. Kamimura, S. Hosoi, J. T. Okada, and K. Kimura, Z. Kristallogr. **224**, 79 (2009).
[16] Y. Takagiwa, T. Kamimura, S. Hosoi, J. T. Okada, and K. Kimura, Z. Kristallogr. **224**, 21 (2009); J. Appl. Phys. **104**, 073721 (2008).
[17] J. M. Dubois, S. S. Kang, P. Archembault, and B. Colleret, J. Mater. Res. **8**, 38 (1993).
[18] J. T. Okada, T. Hamamatsu, S. Hosoi, T. Nagata, and K. Kimura, J. Appl. Phys. **101**, 103702 (2007).
[19] T. Nagata, K. Kirihara, and K. Kimura, J. Appl. Phys. **94**, 6560 (2003).
[20] T. Takeuchi, T. Otagiri, H. Sakagami, T. Kondo, and U. Mizutani, in *Quasicrystals*, MRS Symposia Proceedings No. 805 (Materials Research Society, Boston, 2004), p. 105.
[21] G. D. Mahan and J. O. Sofo, Proc. Natl. Acad. Sci. U.S.A. **93**, 7436 (1996).
[22] U. Mizutani, *Introduction to the Electron Theory of Metals* (Cambridge University Press, Cambridge, 2001).
[23] R. Escudero, J. C. Lasjaunias, Y. Calvayrac, and M. Boudard, J. Phys.: Condens. Matter **11**, 383 (1999).
[24] R. Widmer, P. Gröning, M. Feuerbacher, and O. Gröning, Phys. Rev. B **79**, 104202 (2009).
[25] E. Maciá, Appl. Phys. Lett. **77**, 3045 (2000).
[26] E. Maciá, J. Appl. Phys. **93**, 1014 (2003).
[27] E. Maciá, Phys. Rev. B **69**, 132201 (2004).
[28] E. Maciá, Phys. Rev. B **70**, 100201(R) (2004).
[29] Z. M. Stadnik, D. Purdie, Y. Baer, and T. A. Lograsso, Phys. Rev. B **64**, 214202 (2001); Z. M. Stadnik, in *Physical Properties of Quasicrystals*, Springer Series in Solid-State Physics Vol. 126, edited by Z. M. Stadnik (Springer, Berlin, 1999), p. 257.
[30] C. V. Landauro, E. Maciá, and H. Solbrig, Phys. Rev. B **67**, 184206 (2003).
[31] T. Klein, O. G. Symko, D. N. Davydov, and A. G. M. Jansen, Phys. Rev. Lett. **74**, 3656 (1995).
[32] D. N. Davydov, D. Mayou, C. Berger, C. Gignoux, A. Neumann, A. G. M. Jansen, and P. Wyder, Phys. Rev. Lett. **77**, 3173 (1996).
[33] X. P. Tang, E. A. Hill, S. K. Wonnell, S. J. Poon, and Y. Wu, Phys. Rev. Lett. **79**, 1070 (1997).
[34] T. Fujiwara, in *Physical Properties of Quasicrystals*, Springer Series in Solid-State Physics Vol. 126, edited by Z. M. Stadnik (Springer, Berlin, 1999), p. 169.
[35] G. Trambly de Laissardière, Z. Kristallogr. **224**, 123 (2009).
[36] E. S. Zijlstra and S. K. Bose, Phys. Rev. B **67**, 224204 (2003).
[37] C. Janot and M. de Boissieu, Phys. Rev. Lett. **72**, 1674 (1994); C. Janot, Phys. Rev. B **53**, 181 (1996).
[38] G. Trambly de Laissardière and D. Mayou, Phys. Rev. B **55**, 2890 (1997); G. Trambly de Laissardière, S. Roche, and D. Mayou, Mater. Sci. Eng., A **226-228**, 986 (1997).
[39] H. Solbrig and C. V. Landauro, Physica B **292**, 47 (2000).
[40] E. Maciá, T. Takeuchi, and T. Otagiri, Phys. Rev. B **72**, 174208 (2005).
[41] E. Maciá and J. Dolinšek, J. Phys.: Condens. Matter **19**, 176212 (2007).
[42] E. Maciá, Phys. Rev. B **79**, 245112 (2009).
[43] T. Takeuchi, Z. Kristallogr. **224**, 35 (2009).
[44] E. Maciá, Phys. Rev. B **69**, 184202 (2004).
[45] C. V. Landauro and H. Solbrig, Mater. Sci. Eng., A **294-296**, 600 (2000); Physica B **301**, 267 (2001).
[46] S. Roche and T. Fujiwara, Phys. Rev. B **58**, 11338 (1998).
[47] S. Roche and D. Mayou, Phys. Rev. Lett. **79**, 2518 (1997).
[48] P. A. Thiel and J. M. Dubois, Nature (London) **406**, 570 (2000).
[49] E. Maciá and F. Domínguez-Adame, Phys. Rev. Lett. **76**, 2957 (1996); E. Maciá, Phys. Rev. B **60**, 10032 (1999).
[50] K. Kirihara, T. Nagata, K. Kimura, K. Kato, M. Takata, E. Nishibori, and M. Sakata, Phys. Rev. B **68**, 014205 (2003).
[51] M. Takeda, R. Tamura, Y. Sakairi, and K. Kimura, in *Proceedings of the Sixth International Conference on Quasicrystals*, edited by S. Takeuchi and T. Fujiwara (World Scientific, Singapore, 1998), p. 571; Y. Sakairi, M. Takeda, R. Tamura, K. Edagawa, and K. Kimura, Mater. Sci. Eng., A **294-296**, 519 (2000).
[52] Q. Lin and J. D. Corbett, *Controlled Assembly and Modification of Inorganic Systems* (Springer-Verlag, Berlin, 2009), pp. 1–39.
[53] Q. Lin and J. D. Corbett, J. Am. Chem. Soc. **127**, 12786 (2005); **129**, 6789 (2007).